THE JOURNAL OF PHYSICAL CHEMISTRY B

Article

Cite This: J. Phys. Chem. B 2018, 122, 5487−5499

pubs.acs.org/JPCB

Exploring the Underlying Mechanisms of the *Xenopus laevis* Embryonic Cell Cycle

Kun Zhang[†] and Jin Wang*[,†,‡]

[†]State Key Laboratory of Electroanalytical Chemistry, Changchun Institute of Applied Chemistry, Chinese Academy of Sciences, Changchun, Jilin, 130022, P.R. China

[‡]Department of Chemistry and Physics, Department of Applied Mathematics, Stony Brook University, Stony Brook, New York 11794, United States

ABSTRACT: The cell cycle is an indispensable process in proliferation and development. Despite significant efforts, global quantification and physical understanding are still challenging. In this study, we explored the mechanisms of the *Xenopus laevis* embryonic cell cycle by quantifying the underlying landscape and flux. We uncovered the Mexican hat landscape of the *Xenopus laevis* embryonic cell cycle with several local basins and barriers on the oscillation path. The local basins characterize the different phases of the *Xenopus laevis* embryonic cell cycle, and the local barriers represent the checkpoints. The checkpoint mechanism of the cell cycle is revealed by the landscape basins and barriers. While landscape shape determines the stabilities of the states on the oscillation path, the curl flux force determines the stability of the cell cycle flow. Replication is fundamental for biology of living cells. We quantify the input energy (through the entropy production) as the thermodynamic requirement for initiation and sustainability of single cell life (cell cycle). Furthermore, we also quantify curl flux originated from the input energy as the dynamical requirement for the emergence of a new stable phase (cell cycle). This can provide a new quantitative insight for the origin of single cell life. In fact, the curl flux originated from the energy input or nutrition supply determines the speed and guarantees the progression of the cell cycle. The speed of the cell cycle is a hallmark of cancer. We characterized the quality of the cell cycle by the coherence time and found it is supported by the flux and energy cost. We are also able to quantify the degree of time irreversibility by the cross correlation function forward and backward in time from the stochastic traces in the simulation or experiments, providing a way for the quantification of the time irreversibility and the flux. Through global sensitivity analysis upon landscape and flux, we can identify the key elements for controlling the cell cycle speed. This can help to design an effective strategy for drug discovery against cancer.

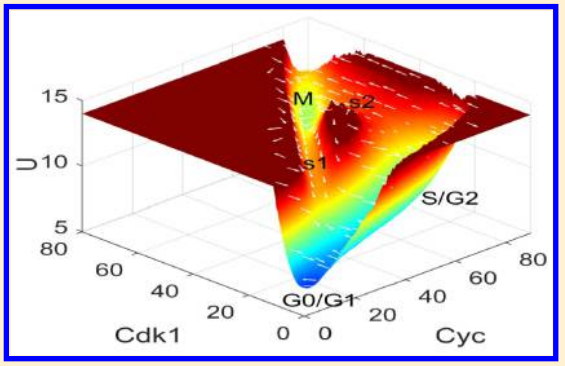

INTRODUCTION

The cell cycle is a periodic process in the biological cell that duplicates its own components and divides into two daughter cells. In this process, the genetic material containing DNA molecule is accurately replicated, and then, the two copies are separated into the daughter cells during division. Exploring the mechanism of the cell cycle is important for understanding cell growth, development, reproduction, and death.[1−4] The complete cell cycle is composed of four phases: the synthesis of DNA (S phase), mitosis (M phase), and the intervening phase G1 and G2. The M phase is divided into four subphases: prophase, metaphase, anaphase, and telophase. Sometimes, the cell can enter into a state of quiescence called the G0 phase in which the cell temporarily or reversibly stops dividing. To ensure the proper progression of the cell division, the cell cycle checkpoints control the ordering of the cell cycle. This leads to the starting of each phase dependent on the completion of the previous one. It is now believed that the cell cycle process is tightly controlled by the underlying gene regulatory network. With the increasing understanding of the biology, mathematical models have been proposed to uncover the mechanisms.[2,5,6] The key of these models is the activity of cyclin-dependent kinases (CDKs) and their associated cyclin protein, which jointly dominate the process of the cell cycle.[7]

It is still challenging to see exactly how the underlying gene regulatory network controls the cell cycle progress because of the complexity of the network. In addition, there are intrinsic fluctuations from the finite number of molecules and extrinsic fluctuations from inhomogeneous environments in the living cells.[8,9] Therefore, the stochastic nature must be considered in studying the cell cycle.[10−15] Although the stochastic nature of the gene regulatory network has been studied, it is still challenging to have global quantifications and physical explanations for the cell cycle to reveal its underlying mechanisms.

Special Issue: Ken A. Dill Festschrift

Received: November 30, 2017
Revised: January 2, 2018
Published: January 8, 2018

DOI: 10.1021/acs.jpcb.7b11840
J. Phys. Chem. B 2018, 122, 5487−5499

In this work, we explore the mechanisms of the *Xenopus laevis* embryonic cell cycle controlled by the underlying gene regulatory network. We do so by the quantifications of the underlying landscape and the flux.[16−21] The different gene expression patterns in the cell cycle can be represented in the state space of the underlying gene regulatory network. There are many such states in the state space. Not every state is equally probable. The weight of occurrence for every gene expression pattern can be described by the probability distribution in state space. The higher probability means a higher chance of appearance which can be observed in the experiments. The specific functional states or phases of the cell correspond to the specific gene expression patterns, often with higher probabilities (or lower potential valleys) on the landscape. By quantifying the topography of the potential landscape through the barrier heights and kinetics between different basins as well as the underlying curl flux, we can identify the driving force of the cell cycle and explore the global stabilities of the oscillation states and the flow of the *Xenopus laevis* embryonic cell cycle. Furthermore, we can quantify the energy dissipation of the cell cycle and investigate the origin of the curl flux and the speed of the *Xenopus laevis* embryonic cell cycle. We show that cell replication cannot proceed without energy input. Therefore, energy input is a necessary condition for replication and life. We quantify the input energy (through the entropy production) as the thermodynamic energy requirement for initiation and sustainability of single cell life. We also quantify the curl flux originated from the energy input as the driving force for the dynamical requirement of the emergence of a new stable phase (cell cycle). This can provide a new quantitative insight for the origin of single cell life. By exploring the relationship between the entropy production rate (energy cost) as well as the curl flux and speed of the cell cycle, we can understand this at the quantitative level. We characterize the quality of the cell cycle by the coherence time and found it is supported by the flux and energy cost. We are also able to quantify the degree of time irreversibility by the cross correlation function forward and backward in time from the stochastic traces in the simulation or experiments. This provides a way for the quantification of time irreversibility and the flux. Through the global sensitivity analysis of the regulation parameters on the landscape topography in terms of the barrier height, the curl flux, and the speed of cell cycle, we can identify the key regulatory elements required for the normal function of the frog cell cycle. Some are consistent with the previous experimental studies. Others are the predicted ones waiting to be tested. The cell cycle speed is a hallmark of cancer. The cancer cells have a much faster speed of cell cycle than the normal cells. We can identify certain predicted key regulatory elements as the potential targets for controlling the cell cycle speed against cancer.

MATERIALS AND METHODS

The dynamics of the gene regulatory network can often be described by a set of ordinary different equations. The cell cycle control dynamics realized by the underlying gene regulatory network can be described by ODEs. However, the deterministic description is not complete for the fluctuating environments of the gene regulatory networks. The intrinsic statistical fluctuations from the finite number of molecules inside of the cell and external fluctuations from cellular environments have significant impacts on the network dynamics. In bacterial cells, the intrinsic statistical fluctuations from the finite number of molecules in the cells can be significant. For the frog cell we study here, the number of molecules is large in the cell so the intrinsic statistical fluctuations from the molecular numbers are expected to be small. Most of the fluctuations here can be captured by the extrinsic fluctuations rather than the intrinsic fluctuations. We only consider extrinsic fluctuations in this study which can be added to the deterministic concentration dynamical equations, resulting in the stochastic concentration dynamical equations. Therefore, it is necessary for the dynamics of the regulatory network to be formulated as the stochastic different equations with the noise $\frac{d\mathbf{x}}{dt} = \mathbf{F}(\mathbf{x}) + \eta$, where $\mathbf{x}$ is the concentration or expression levels of the substance and $\mathbf{F}(\mathbf{x})$ is the driving force of the system. η is the Gaussian white noise term with zero mean, and its autocorrelation function is given as $\langle \eta(t)\eta(0)\rangle = 2D\delta(t)$. D is the diffusion coe cient. This characterizes the intensity of the intrinsic and cellular environmental fluctuations. The process is similar to Brownian dynamics, and the diffusion coe cient can be dependent on the concentration.

The time evolution of the expression or concentration dynamics is not deterministic because of the stochastic nature. A more appropriate quantitative description can be obtained by the probability distribution. One can do statistical analysis and calculate out the probability distribution at steady state from the simulated trajectories of the underlying stochastic dynamics. On the other hand, the probability evolution follows the diffusion equations for the continuous case.[22] The equation is also called the Fokker−Plank equation which can be written in the form of probability conservation: $\partial P/\partial t + \quad \cdot J = 0$, where J is defined as the probability flux, $J = FP - D \quad P$. The equation states that the increase or decrease of the local probability is equal to the net input flux. When the divergence of the probability flux $\mathbf{J}_{ss}$ is zero ($\quad \cdot J = 0$), the nonequilibrium system attains the steady state. We can solve out the steady state probability distribution P_{ss} from the Fokker−Plank equation. In the 2-variable system, we constructed the landscape by directly solving the Fokker−Plank equation and obtained the steady state distribution. For the 33-variable system, we performed the statistical joint histogram analysis and computed the 2-variable marginal probability distribution at steady state from the long time simulated trajectories of the underlying stochastic Langevin dynamics for the protein concentrations or the gene expressions. We define the potential $U = -\ln P_{ss}$ which resembles the Boltzmann law under equilibrium conditions. If the local flux is equal to zero, then the detailed balance condition is satisfied and the system is in equilibrium state. When the local flux is not equal to zero, the detailed balance is broken and the system is in nonequilibrium steady state; we see that $\mathbf{F} = -D\cdot \quad U + \mathbf{J}_{ss}/P_{ss}$. Thus, we have decomposed the force driving the dynamics of the system into two terms. The first is related to the gradient of the potential U, and the second term is the steady state probability flux $\mathbf{J}_{ss}$ (velocity current) divided by the steady-state probability P_{ss} (density). The steady state flux is divergent free at steady state and therefore rotational termed as curl flux. The nonequilibrium dynamics is analogous to a moving electron in the electric and magnetic field.

The nonequilibrium system is an open system with exchanges in energy, materials, and information to the environments. The system will generate energy consumption and dissipation. The dissipation as a global physical characteristic can be used to measure the degree of the nonequilibrium away from the equilibrium. The energy dissipation is associated

DOI: 10.1021/acs.jpcb.7b11840
J. Phys. Chem. B 2018, 122, 5487−5499

with the entropy production rate in the steady state of the nonequilibrium system.[23,24] The system entropy can be written as $S = -\int P(\mathbf{x}, \mathbf{t}) \ln \mathbf{P}(\mathbf{x}, \mathbf{t})\, d\mathbf{x}$. By differentiating the above expression, the change rate of the system entropy can be formulated as follows: $\dot{S} = \int (\mathbf{J}\cdot\mathbf{D}^{-1}\cdot\mathbf{J})/\mathbf{P}\, d\mathbf{x} - \int (\mathbf{J}\cdot\mathbf{D}^{-1}\cdot(\mathbf{F} - \nabla\cdot\mathbf{D}))\, d\mathbf{x}$, where $\int (\mathbf{J}\cdot\mathbf{D}^{-1}\cdot\mathbf{J})/\mathbf{P}\, d\mathbf{x} = \mathbf{e}_p = \dot{\mathbf{S}}_{tot}$ is the entropy production rate (EPR). It represents the total entropy change rate (including both system and environment). $\int (\mathbf{J}\cdot\mathbf{D}^{-1}\cdot(\mathbf{F} - \nabla\cdot\mathbf{D}))\, d\mathbf{x} = \mathbf{h}_d = \dot{\mathbf{S}}_{env}$ is the rate of the heat dissipation or the entropy change rate from the environment. When the nonequilibrium system is in a steady state, the change rate of the system entropy $\dot{S}$ is equal to zero. Therefore, the entropy production rate is equal to the heat dissipation from the environment in the steady state. According to the equation, the energy dissipation quantified by entropy production e_p and h_d is associated directly with the curl flux $\mathbf{J}$. The equation can also be written as $\dot{S}_{tot} = \dot{S} + \dot{S}_{env}$. This gives the first law of nonequilibrium thermodynamics. The entropy production is always larger or equal to zero. This gives the second law of nonequilibrium thermodynamics.[23]

RESULTS AND DISCUSSION

Cell Cycle Model. Mathematical models of the cell cycle have been proposed.[1,2,19,25−29] In this study, we explore the *Xenopus laevis* embryonic cell cycle network. The *Xenopus* eggs are used extensively in cell cycle studies because they can grow very large without dividing and can easily be manipulated. Before fertilization, the eggs stop at the metaphase of meiosis II (haploid complement of replicated chromosomes aligned on the spindle). After fertilization, the *Xenopus* egg finishes meiosis and then achieves its first mitotic cell cycle. The first mitotic cycle takes about 85 min, and the subsequent 11 cycles are about 30 min each. They are synchronous mitotic cycles. These cell cycles are not size-controlled, and the cells get smaller at each division. After the 12th division, the period of the somatic cell becomes much slower.[30] The cell cycles oscillate between S and M phases with G1 and G2 phases significantly shortened. The *Xenopus laevis* embryonic cell cycle is quite different from the yeast cell cycle. Yeast cells are much smaller and can maintain a constant cell-size distribution by cell-size checkpoints in G1 and/or G2. The budding yeast divides by first forming a bud that starts and grows steadily during the S and G2 phases, and finally leaves its mother after mitosis.

The core design of biological oscillators invariably consists of a negative feedback. The gene regulatory network often involves both positive and negative feedback loops. With both positive and negative feedback loops, the oscillators generated can provide a wider range of period and robust amplitude. The resulting dynamics behaves like a relaxation oscillator that is established on a hysteretic switch. The hysteretic response of the Cdk1/Cdc25/Wee1 feedback loop has been shown in the experimental studies of *Xenopus* extracts.[30] Moreover, The larger number of molecules and ultrasensitive negative feedback in the frog cell can resist intrinsic stochastic noise. We introduce a two-gene model that includes fewer adjustable parameters. The simpler model is beneficial to analyze the general nature and compare to other activator−repressor circuits. This cell cycle gene circuit was proposed earlier.[25] The model was represented by the following two equations

$$\frac{d}{dt}\mathrm{Cyc} = k_s - k_{deg}\mathrm{Cyc}$$

$$\frac{d}{dt}\mathrm{Cdk1} = k_s + k_{cdc}(\mathrm{Cyc} - \mathrm{Cdk1}) - k_{Wee1} \times \mathrm{Cdk1} - k_{deg}\mathrm{Cdk1}$$

where the first equation describes the synthesis and degradation of the moitotic cyclins. k_s is a rate constant of cyclin synthesis, k_{deg} is a rate constant of cyclin degradation which varied with the activity of Cdk1 and can be described by the Hill function: $k_{deg} = a_{deg} + b_{deg}\frac{\mathrm{Cdk1}^{n_{deg}}}{\mathrm{EC50}_{deg}^{n_{deg}} + \mathrm{Cdk1}^{n_{deg}}}$. The second equation describes the production of active Cdk1. The parameter k_{cdc} represents the production rate of protein Cdc25C which can activate Cdk1 by removing phosphate. The parameter k_{Wee1} denotes the production rate of protein kinase Wee1A which can repress the active Cdk1. Both k_{cdc} and k_{Wee1} are the functions of the active Cdk1 concentration. Their steady-state response was determined by experimental studies and can be approximated by the Hill functions: $k_{cdc} = a_{cdc} + b_{cdc}\frac{\mathrm{Cdk1}^{n_{cdc}}}{\mathrm{EC50}_{cdc}^{n_{cdc}} + \mathrm{Cdk1}^{n_{cdc}}}$, $k_{Wee1} = a_{Wee1} + b_{Wee1}\frac{\mathrm{EC50}_{Wee1}^{n_{Wee1}}}{\mathrm{EC50}_{Wee1}^{n_{Wee1}} + \mathrm{Cdk1}^{n_{Wee1}}}$.

This two-dimensional model assumed that there is no time lag between the activation of Cdk1 and regulation of cyclin degradation. The activation of APC/CCdc20 depends on Cdk1-dependent phosphorylation events, and the same multistep mechanism can also account for the observed time delay. Thus, the observed steady-state and dynamic behaviors of the negative feedback loop are consistent with a multistep phosphorylation/activation mechanism.[25] Considering the realistic time lag into the negative feedback loop, the model can be expressed with the following equation

$$\frac{d}{dt}\mathrm{Cyc} = k_s - (a_{deg} + b_{deg}\mathrm{APC}_{30})\mathrm{Cyc}$$

$$\frac{d}{dt}\mathrm{Cdk1} = k_s + \left(a_{cdc} + b_{cdc}\frac{\mathrm{Cdk1}^{n_{cdc}}}{\mathrm{EC50}_{cdc}^{n_{cdc}} + \mathrm{Cdk1}^{n_{cdc}}}\right)(\mathrm{Cyc} - \mathrm{Cdk1}) - \left(a_{Wee1} + b_{Wee1}\frac{\mathrm{EC50}_{Wee1}^{n_{Wee1}}}{\mathrm{EC50}_{Wee1}^{n_{Wee1}} + \mathrm{Cdk1}^{n_{Wee1}}}\right) \times \mathrm{Cdk1} - (a_{deg} + b_{deg}\mathrm{APC}_{30})\mathrm{Cdk1}$$

$$\frac{d}{dt}\mathrm{APC}_0 = -k_p\mathrm{Cdk1APC}_0 + k_d\mathrm{APC}_1$$

$$\frac{d}{dt}\mathrm{APC}_1 = k_p\mathrm{Cdk1APC}_0 - k_d\mathrm{APC}_1 - k_p\mathrm{Cdk1APC}_1 + k_d\mathrm{APC}_2$$

$$\frac{d}{dt}\mathrm{APC}_2 = k_p\mathrm{Cdk1APC}_1 - k_d\mathrm{APC}_2 - k_p\mathrm{Cdk1APC}_2 + k_d\mathrm{APC}_3$$

$$\cdots$$

$$\frac{d}{dt}\mathrm{APC}_{29} = k_p\mathrm{Cdk1APC}_{28} - k_d\mathrm{APC}_{29} - ck_p\mathrm{Cdk1APC}_{29} + \frac{1}{c}k_d\mathrm{APC}_{30}$$

$$\frac{d}{dt}\mathrm{APC}_{30} = ck_p\mathrm{Cdk1APC}_{29} - \frac{1}{c}k_d\mathrm{APC}_{30}$$

where APC has 31 phosphorylated forms and only the final form is active. The constant c denotes the cooperativity of the phosphorylation and dephosphorylation reactions.

Landscape and Flux of the Cell Cycle System. On the basis of the underlying gene regulatory network, we investigate the associated stochastic dynamics. By following the probabilistic evolution, we can quantify the steady state probability distribution in the expression state space. We found the underlying potential landscape of the limit cycle dynamics of the *Xenopus laevis* embryonic cell cycle has a Mexican hat shape

DOI: 10.1021/acs.jpcb.7b11840
J. Phys. Chem. B 2018, 122, 5487−5499

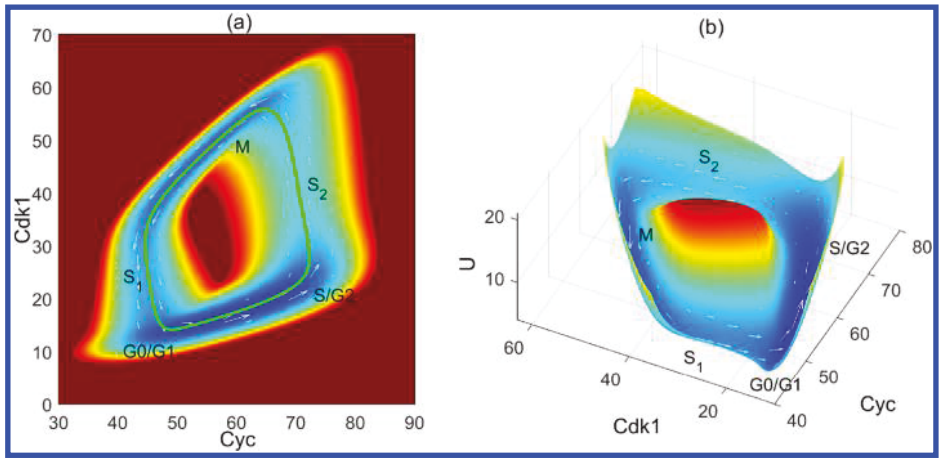

Figure 1. (a) Two-dimensional landscape of the 2-dimension cell cycle model. (b) Three-dimensional landscape of the 2-dimension cell cycle model.

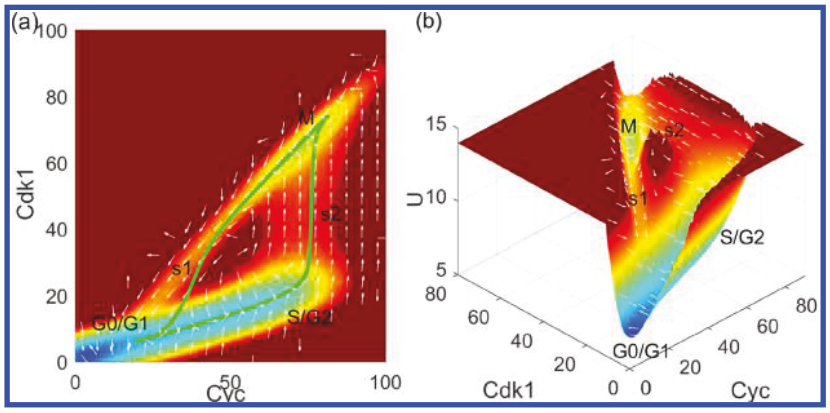

Figure 2. (a) Two-dimensional landscape of the 33-dimension cell cycle model. (b) Three-dimensional landscape of the 33-dimension cell cycle model.

with uneven valleys. Outside the oscillation cycle ring, the dynamics is attracted to the ring mainly by the negative landscape gradient, which guarantees the stability of the states on the oscillation path. Once on the oscillation ring, the driving force for the *Xenopus laevis* embryonic cell cycle is then mainly determined by the curl flux along the cycle along with the impeding force from the local basins and barriers on the cycle. We found a few local basins and barriers between the basins along the *Xenopus laevis* embryonic cell cycle trajectory. These local basins on the potential landscape reflect the different phases of the *Xenopus laevis* embryonic cell cycle processes. The saddle points between the basins on the landscape quantify the checkpoints of different stages of the *Xenopus laevis* embryonic cell cycle. These quantifications can be used to uncover the checkpoint mechanisms of the *Xenopus laevis* embryonic cell cycle from physical perspectives. Through the global picture via the landscapes and flux on cell cycle progression, we can quantify the global stability and function of the *Xenopus laevis* embryonic cell cycle. To complete the cell cycle progression, the cell cycle process has to overcome the major barriers by su cient driving force. In other words, the *Xenopus laevis* embryonic cell cycle progression must prepare adequately to pass through each checkpoint. The curl flux provides such a driving force. While the curl force drives the cycle, because the cycling trajectory is not in a plane, the gradient force also has an impact locally impeding and helping the cycle, depending on the location. Due to the impacts of the local gradient force on the cell cycle path, only su cient curl force can guarantee stable cycle flow against the local landscape barriers. We can also estimate the energy dissipation required for maintaining the *Xenopus laevis* embryonic cell. We found it is correlated with the curl flux. Therefore, the *Xenopus laevis* embryonic cell cycle process requires the energy input through nutrition supply. We further found the period and coherence of the *Xenopus laevis* embryonic cell cycle is strongly correlated with curl flux.

Figure 1a shows the two-dimensional potential landscape of the 2-variable *Xenopus laevis* embryonic cell cycle model. We find the landscape has two valley basins and two saddle points. The bottom basin has a long and narrow shaped valley. It represents the G0/G1 phase and S/G2 phase on each side of the valley, respectively. The saddle point s2 along the cell cycle path is the G2 checkpoint, which can guarantee that DNA replication is achieved before reaching the next phase M. The top basin represents that the cell attains the M phase. When a cell matures and the division occurs, the cell goes through saddle point s1 from the phase M back to the G0/G1 phase. The saddle point s1 is the M checkpoint. Figure 1b show the three-dimensional potential landscape of the 2-variable *Xenopus laevis* embryonic cell cycle model. The figure further represents the progression of the cell cycle by the landscape and the flux (white arrow).

Figure 2a shows the two-dimensional landscape of the more sophisticated 33-variable cell cycle model. The white arrow is the probability curl flux. The negative gradient of the potential landscape attracts the system to the oscillation path. On the oscillation path, the curl flux guarantees the stable cell cycle

DOI: 10.1021/acs.jpcb.7b11840
J. Phys. Chem. B 2018, 122, 5487−5499

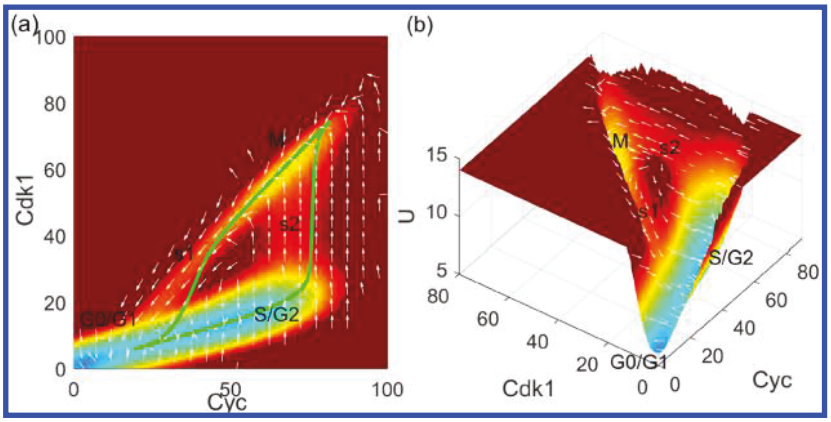

Figure 3. (a) Two-dimensional landscape of the 33-dimension cell cycle model with parameter b_{deg} = 0.18. (b) Three-dimensional landscape of the 33-dimension cell cycle model with parameter b_{deg} = 0.18.

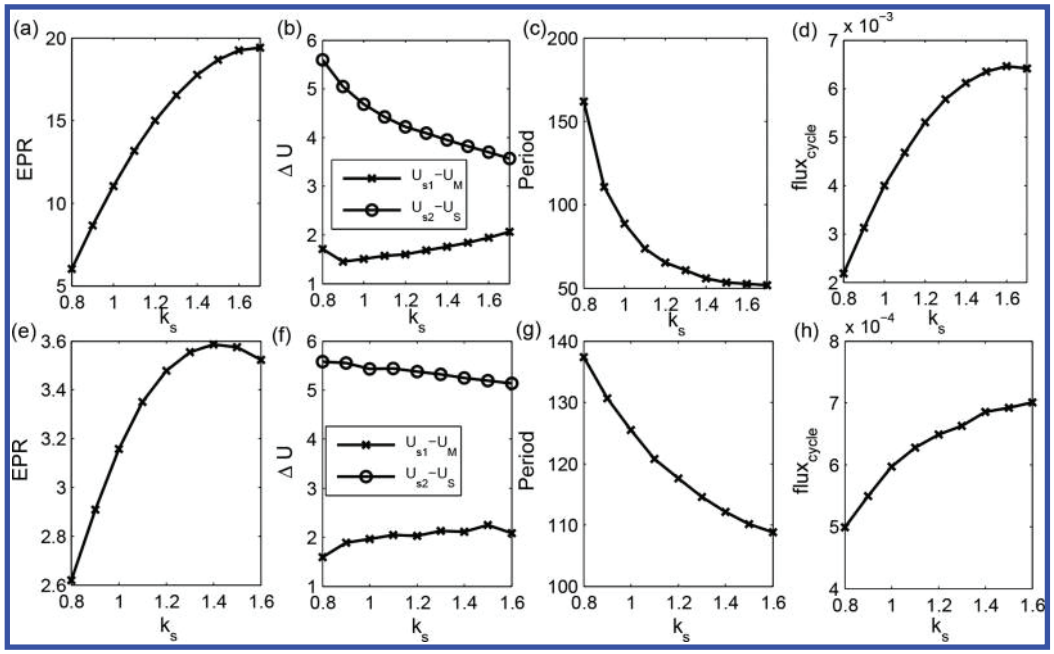

Figure 4. (a, e) Entropy production rate with different k_s. (b, f) Barrier height versus parameter k_s. (c, g) The period (units: minutes) with different k_s. (d, h) The integral of flux along the limit cycle $J\,dl/dl$ versus parameter k_s. (top) 2-Dimension model; (bottom) 33-dimension model.

flow. The landscapes show a similar process of mitosis with both the 2-variable and 33-variable models, but the total cyclin and active Cdk1 of the G0/G1 phase are lower in the 33-variable model. We also see in the 33-variable model that there is a sharp increase in CDK1 from S/G2 (together with G0/G1 under this parameter range) to the M phase and there is also a sharp decrease of CDK1 from the M phase back to the G0/G1 phase in contrast to the 2-variable model. Figure 2b show the three-dimensional potential landscape of the 33-variable *Xenopus laevis* embryonic cell cycle model.

By comparisons, we find some differences of the two landscapes between the 2-variable and 33-variable (multistep phosphorylation) models. The landscape of the 2-variable model has less range of variability for the expressions of cyclin and Cdk1 than the 33-variable model. In other words, when we consider the realistic time delays by a multistep phosphorylation/activation mechanism, the amplitude and the period of oscillations can be varied and oscillation stability is more ensured. The extracts of early *Xenopus* eggs and embryos lack an obvious cell cycle checkpoint that keeps anaphase from occurring before spindle assembly is finished.[31] However, the time lag can ensure that the Cdk1-dependent mitotic processes are achieved before the Cdk1 inactivation and mitotic exit occur (from M back to G0/G1). On the landscape of the 33-variable model, the basin of mitotic phase is narrower than that of the 2-variable model. This can guarantee the completion of the mitotic phase before the Cdk1 inactivation. We compare the landscapes of the *Xenopus laevis* embryonic cell cycle and the mammalian cell cycle.[26] We can see the landscape of the mammalian cell cycle has a certain similarity to the landscape of the 2-variable model here. Both mitotic areas from the 2-variable model for frogs and the model for the mammalian cell cycle[26] have no obvious barrier as the threshold for the mitotic completion (from M back to G0/G1). One can see the nature of the time lag illustrated in the 33-variable model for multistep phosphorylation as the effective spindle assembly checkpoint in the *Xenopus laevis* embryonic cell cycle.

Figure 3 shows the two- and three-dimensional potential landscapes of the 33-variable *Xenopus laevis* embryonic cell cycle network with different parameters from Figure 2. In this

DOI: 10.1021/acs.jpcb.7b11840
J. Phys. Chem. B 2018, 122, 5487−5499

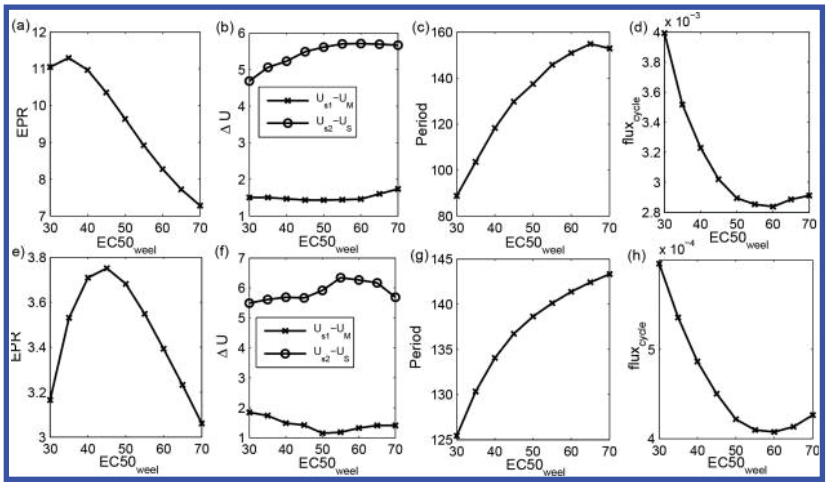

Figure 5. (a, e) Entropy production rate with different $EC50_{Wee1}$. (b, f) Barrier height versus parameter $EC50_{Wee1}$. (c, g) The period (units: minutes) with different $EC50_{Wee1}$. (d, h) The integral of flux along the limit cycle $\int J\,dl/dl$ versus parameter $EC50_{Wee1}$. (top) 2-Dimension model; (bottom) 33-dimension model.

parameter setting, the G0/G1 phase and S/G1 phase are in different attractor basins. This gives a G1 checkpoint between the G0/G1 phase and the S phase.

The Effects of Some Parameters for the Cell Cycle System. To study the energy cost of the cell cycle processes, we compute the entropy production rate with different parameters. As shown in Figure 4a, the entropy production rate increases with the increase of cyclin synthesis rate. This result states that the increasing of the cyclin synthesis rate requires more energy or nutrition supply. In Figure 4b, we show the changes of the two barrier heights with different cyclin synthesis rate constants. One is the barrier height between the saddle s2 and the bottom basin. It characterizes the G2 checkpoint and quantifies the degree of di culty of the cell cycle from the G2 phase to the M phase. The other is the barrier height between the saddle s1 and the top basin. It denotes the degree of di culty of the cell cycle from the M phase back to the G0/G1 phase. We find the first barrier through s1 decreases with increasing cyclin synthesis rates. It indicates the division of a cell is likely to be easier under this condition. The latter barrier increases with increasing synthesis rate. It states that a cell in the S/G2 phase becomes more di cult to get to the M phase through the G2 checkpoint. In Figure 4c, we calculated the period of the cell cycle and find the period decreases with increasing cyclin synthesis rates. The period can reflect how fast the cell cycle oscillates and its growth rate. Thus, the result implies that the increasing cyclin synthesis rate can accelerate the cell cycle and its growth.[32] In Figure 4d, we computed the integral of flux along the limit cycle with different cyclin synthesis rates. We find the integral of flux increases with the cyclin synthesis rate. This reflects that the flux strengthens upon increasing synthesis rate. The flux and the entropy production rate have the same tendency with respect to cyclin synthesis rates. Therefore, the flux of the cell cycle is closely related to the entropy production rate. With increasing cyclin synthesis rate, the *Xenopus laevis* embryonic cell cycle has a stronger flux and a higher entropy production rate. This will consume more energy or nutrition supply. Meanwhile, the cell cycle from maturation to division becomes faster. It is worthwhile to notice that the barrier height and flux together determine the dynamics of the cell cycle such as cycle speed or period. Even though the barrier is higher between the S/G2 and M phases, the flux can still drive the cell cycle through the s2 saddle or transition state (G2 checkpoint) with faster speed.[33−35] As shown in Figure 4e−h, similar conclusions can be drawn from the corresponding more sophisticated 33-variable network.

As shown in Figure 5a, the entropy production rate decreases with an increase in the parameter $EC50_{Wee1}$. The parameter is the Hill constant or the half-maximum effective concentration values of Wee1A as the substrate of Cdk1. This result states that the increase of the parameter $EC50_{Wee1}$ leads to less energy cost. In Figure 5b, we show the change of two barrier heights with different parameters in $EC50_{Wee1}$. One is the barrier height between the saddle s2 and the bottom basin. The other is the barrier height between the saddle s1 and the top basin. They denote the degree of di culty in the cell cycle from the current phase to the next phase. We find that the barriers change smoothly with an increase of the parameter $EC50_{Wee1}$. This indicates that changes in this parameter have a moderate impact on the growth and division of a cell under these conditions. In Figure 5c, we calculated the period of the cell cycle and found that the period increases with an increase of this parameter. Therefore, the trend in cell cycle period shows that an increase of the parameter $EC50_{Wee1}$ can decelerate the cell cycle and its growth. In Figure 5d, we computed the integral of the curl flux along the *Xenopus laevis* embryonic cell cycle with different parameters in $EC50_{Wee1}$. We find that the integral of flux declines with the parameter $EC50_{Wee1}$. Similarly, the flux and the entropy production rate have the same tendency under the changes of the parameter $EC50_{Wee1}$. As shown in Figure 5e−h, similar conclusions can be drawn from the 33-variable model of the *Xenopus laevis* embryonic cell cycle.

The Coherence for the Cell Cycle System. The coherence can quantify the stability of the oscillation and measure the degree of persistence of the oscillatory phase.[36] The coherence ξ is defined with the following method. $N(t) = n_1(t)e_1 + n_2(t)e_2$ is a vector at time t. $n_1(t)$ and $n_2(t)$ are the measures of the two variables. $e_1 = (1, 0)$ and $e_2 = (0, 1)$ are the unit vectors. Then, $\phi(t)$ is the angle between $N(t)$ and $N(t + \tau)$, where τ is smaller than the deterministic period and larger than the fast fluctuations. The coherence ξ can be obtained, $\xi = \frac{2\sum_i \theta(\phi(t))\phi(t)}{\sum_i |\phi(t)|} - 1$, where $\theta(\phi) = 0$ when $\phi(t)$ 0 and

DOI: 10.1021/acs.jpcb.7b11840
J. Phys. Chem. B 2018, 122, 5487−5499

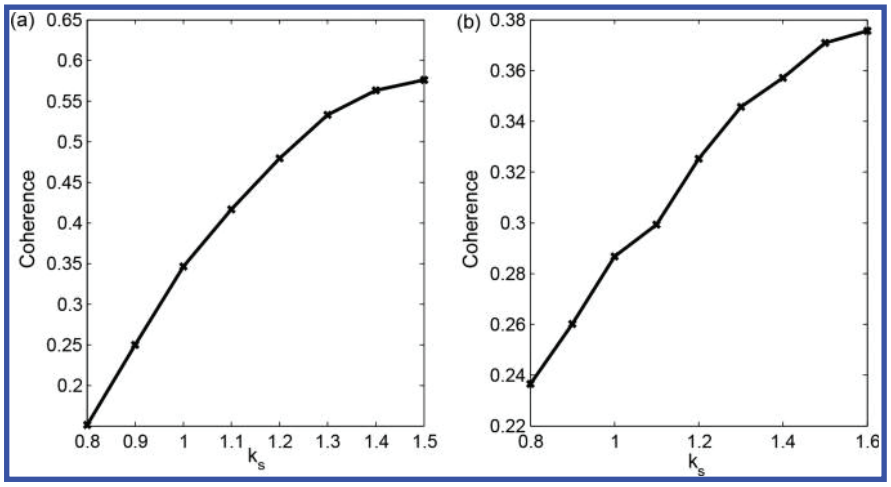

Figure 6. (a) Coherence versus parameter k_s with the 2d model. (b) Coherence versus parameter k_s with the 33d model.

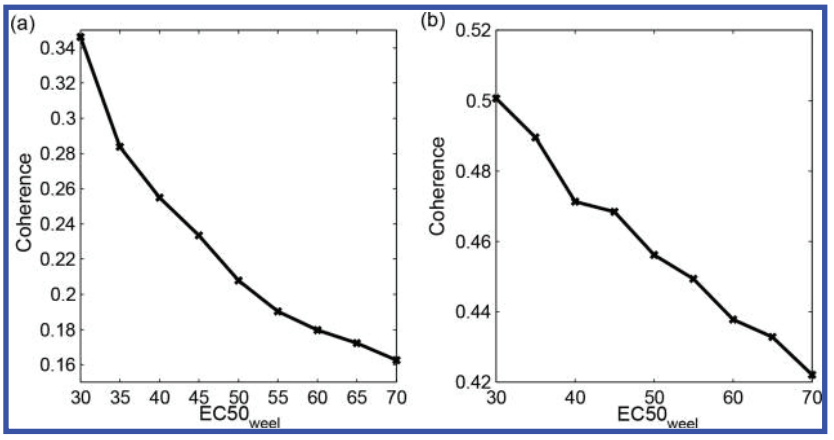

Figure 7. (a) Coherence versus parameter $EC50_{Wee1}$ with the 2d model. (b) Coherence versus parameter $EC50_{Wee1}$ with the 33d model.

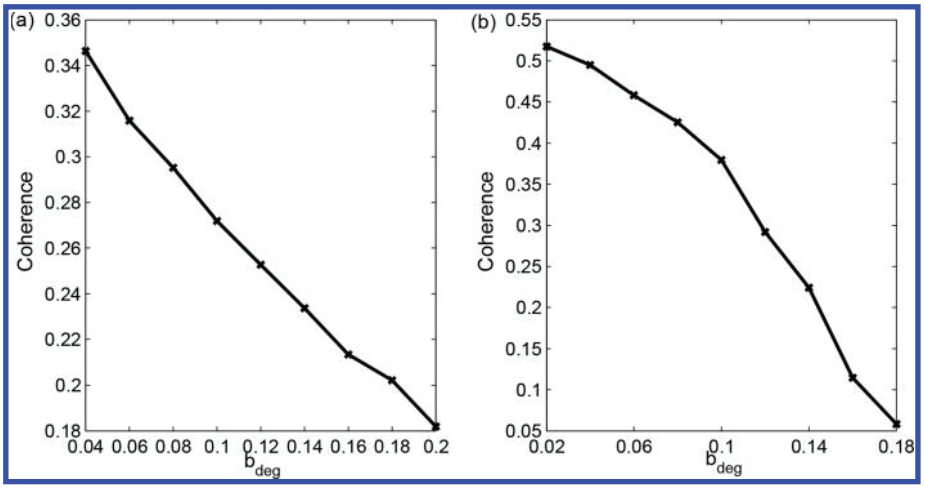

Figure 8. (a) Coherence versus parameter b_{deg} with the 2d model. (b) Coherence versus parameter b_{deg} with the 33d model.

$\theta(\phi) = 1$ when $\phi(t) > 0$, and sums contain every time step of the trajectory. ξ 0 indicates that the system moves stochastically with no preferential direction along the oscillation path. If ξ is close to 1, the oscillation is mostly coherent, since there is a definite direction for the next movement to follow. The more periodic the evolution, the larger the coherence ξ.

In Figure 6, we plot the relationship between the cyclin synthesis rate and the coherence. We find that the coherence increases with the increase of synthesis rate. Meanwhile, we know the flux also becomes stronger with increasing synthesis rate. This states that the enhancement of the flux can improve the stability and coherence of the periodic oscillation and the persistence of the cell cycle.

In Figure 7, we draw the change of the coherence with the parameter $EC50_{Wee1}$. We find that the coherence declines with an increase of the parameter $EC50_{Wee1}$. Meanwhile, the flux also

DOI: 10.1021/acs.jpcb.7b11840
J. Phys. Chem. B 2018, 122, 5487−5499

becomes weaker with an increase of this parameter. It implies that less flux can decrease the stability of the oscillation flow and reduce the cell cycle speed. Flux is thus crucial for maintaining the cell cycle.

In Figure 8, we draw the change of the coherence with the degradation parameter b_{deg}. We find that the coherence declines with an increase of the parameter b_{deg}. Meanwhile, the flux also become weaker with an increase of the degradation parameter b_{deg}. Flux is important for the stability of the oscillation flow and the maintaining of the cell cycle.

The Relationship among the Entropy Production Rate, the Flux, and the Period: The Implication of the Origin of Single Cell Life. In Figure 9, we show the change of the entropy production rate (EPR is defined in the Materials and Methods) with the flux by an example of parameter k_s. We find the EPR increases with the increase of the flux of limit cycle. This indicates that the energy cost of the system is closely related to the flux of the cell cycle. In fact, the thermodynamic energy supply guarantees the emergence of the flux for driving the cell cycle dynamics.

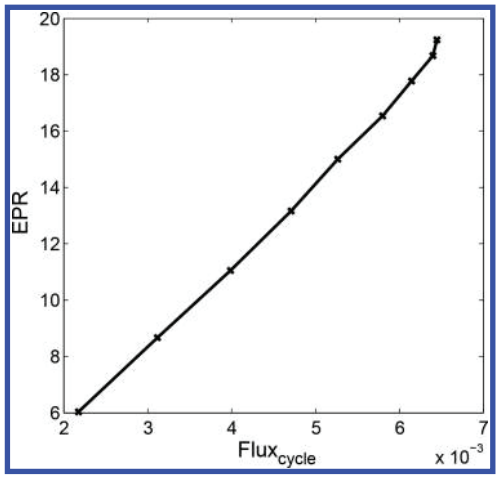

Figure 9. Entropy production rate versus the integral of flux along the limit cycle.

Figure 10a shows that the period of the cell cycle decreases with the increase of the flux. We found that the larger curl flux leads to the faster cell cycle oscillation. In Figure 10b and c, we show the cell cycle period versus EPR and the energy cost per cycle. We see that the cell cycle period monotonically decreases with the increase of both the EPR and the energy cost per cell cycle. The faster (smaller period) the cycle oscillation of the cell growth and division, the more energy per cycle is consumed. This indicates that a su cient supply of the nutrition or energy pump is necessary to drive and accelerate replication such as the cell cycle.

The limit cycle cannot exist without the presence of the curl flux for driving. In fact, the limit cycle is a new "active" phase which cannot emerge spontaneously in the equilibrium systems with detailed balance. As known, the replication is an essential feature of life. From the evolution standpoint, a single cell might be the primordial form of life. The cell cycle governs the life of a single cell. The cell cycle is determined by the limit cycle dynamics. Since the driving force for the cell cycle flow is the curl flux, it is in this sense that we state that the curl flux provides the driving force for the origin of the single cell life at the dynamical level. Since the curl flux comes from the nutrition supply or energy input, we can also state that the energy input is the origin of the life. More precisely, we can state that the energy input as the thermodynamical requirement manifests to produce the curl flux which serves as the driving force for the dynamical emergence of the origin of single cell life as a new phase of active matter.

Global Sensitivity Analysis of Key Genes and Regulations for Cell Cycle. The process of the cell cycle is controlled by the interactions among many genes and gene regulations. To find the key genes and regulatory wirings in the cell cycle network, we perform a global sensitivity analysis of the cell cycle period, the flux integrated along the cell cycle path, and the landscape barrier upon the moderate changes of the genes and wirings. By such global sensitivity analysis, we can identify the key structure elements (genes or gene regulations) or hot spots for the cell cycle network.

Exploring important structural elements of the network (synthesis rate or regulation strengths), we show the results of the global sensitivity analysis in Figure 11. We analyzed the global sensitivity of the flux, the period, and barrier upon changes of the 13 parameters in the *Xenopus laevis* embryonic cell cycle network. We found certain key parameters in the cell cycle network from Figure 11. They are k_s, b_{cdc}, $EC50_{cdc}$, $EC50_{Wee1}$, and n_{Wee1}. k_s represents the synthesis rate of the cyclin. b_{cdc} denotes the maximum rate of phosphorylation of Cdc25C by Cdk1. $EC50_{cdc}$ is the half-maximum effective concentration value of Cdc25C and denotes the concentration demanded of the substrate Cdk1 when Cdc25C achieves half of the activity. $EC50_{Wee1}$ is the half-maximum effective concentration value of Wee1A. n_{Wee1} is the Hill coe cient. It represents the cooperative effect of the Wee1A regulated by

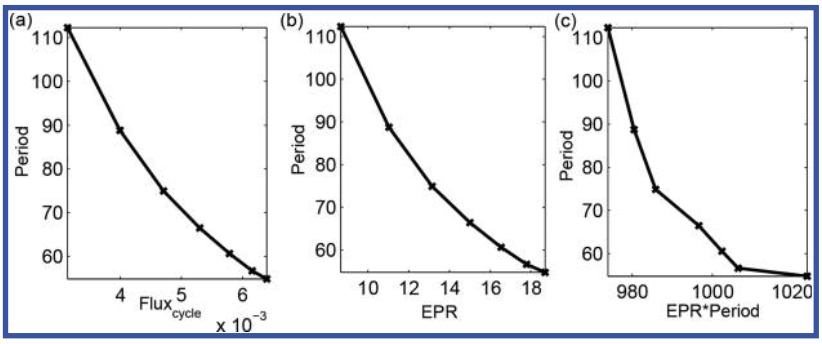

Figure 10. (a) Period versus the integral of flux along the limit cycle. (b) Period versus the entropy production rate. (c) Period versus the entropy production per cycle.

DOI: 10.1021/acs.jpcb.7b11840
J. Phys. Chem. B 2018, 122, 5487−5499

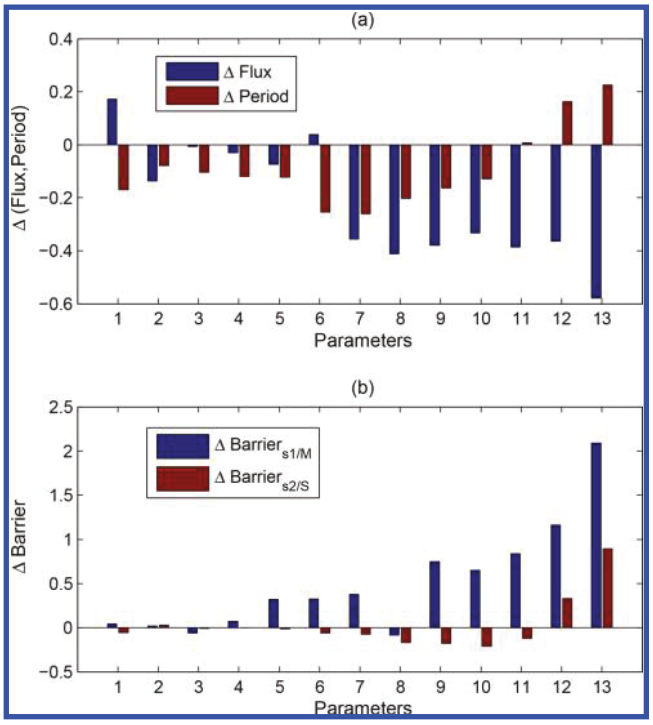

Figure 11. (a) Global sensitivity analysis in terms of the flux and period when parameters are changed. (b) Global sensitivity analysis in terms of the barrier (barrier between s1 and M, barrier between s2 and S) when parameters are changed. The x coordinate (1−13) is corresponding to the 13 parameters: 1, k_s; 2, a_{deg}; 3, b_{deg}; 4, $EC50_{deg}$; 5, n_{deg}; 6, a_{cdc}; 7, b_{cdc}; 8, $EC50_{cdc}$; 9, n_{cdc}; 10, a_{Wee1}; 11, b_{Wee1}; 12, $EC50_{Wee1}$; 13, n_{Wee1}.

Cdk1 and leads to the rapid decrease of the production rate with the increase of the substrate Cdk1.

Figure 11a shows the global sensitivity of the flux along the cell cycle path and the period upon parameter changes. We can see that certain key parameters have more significant effects on the flux or oscillation period. Therefore, the network can have a larger flux and accelerate cell division by adjusting these key parameters. For example, the B-type cyclin is the most important protein in mitosis; its synthesis rate is directly related to the progression of the cell cycle. Therefore, the synthesis rate parameter k_s is one of the key parameters. From Figure 11a, we can also see the increase of the rate can significantly decrease the period and increase the flux. Cdc25C is one of the protein kinases to be phosphorylated by Cdk1. It can reactivate the cyclin−Cdk1 complexes and then accelerate the cell cycle. We also found that the increase of the related maximum synthesis rate b_{cdc} can significantly decrease the period. Wee1A is an early substrate of Cdk1 and inactivates the cyclin−Cdk1 complexes. Therefore, it can repress the cell cycle. From the global sensitivity analysis, we can also see the increase of the related parameter $EC50_{Wee1}$ of Wee1A can increase the period and decrease the flux.

Figure 11b shows the change of the landscape barrier upon parameter change. The $barrier_{s1/M}$ and $barrier_{s2/S}$ respectively characterize the M checkpoint and G1 checkpoint. Therefore, the network can increase (or decrease) the checkpoint barrier by adjusting certain key parameters. For example, Cdc25C proteins are known to control the cell progression from G1 to S phase and G2 to M phase from biologic studies.[37,38] Our analysis shows that the increase of the related maximum synthesis rate b_{cdc} and the half-maximum effective concentration value $EC50_{cdc}$ of Cdc25C can change the activity of Cdc25C and decrease the barrier between s2 and S/G2. This implies that the increase of these regulation parameters can help the cell to go over the G2 checkpoint and accelerate the cell cycle. Wee1A is a key regulator of cell cycle progression and a component of a cell size checkpoint.[39] It can inhibit the entry into mitosis. The related parameter $EC50_{Wee1}$ can significantly influence the activity of Wee1A. From the figure, we see that it increases the barrier between s2 and S/G2, and increases the barrier between s1 and M. Therefore, this can slow down the cell cycle. The above analysis on the key genes and regulations is consistent with the findings of *Xenopus laevis* embryonic cell cycle studies.[40−42] In addition, the current approach can provide predictions for further experimental testing. For example, n_{Wee1} represents the cooperative effect of the Wee1A regulated by Cdk1. From Figure 11, we can see that it significantly increases the period, the barrier between s2 and S/G2, and the barrier between s1 and M. Therefore, we can predict that the increase of ultrasensitivity in the inhibition can significantly slow down the cell cycle. Another predicted key element is the effective positive regulation strength (a_{cdc}, b_{cdc}) of the Cyc on Cdk1 through Cdc25C. The increase of this regulation strength can give a wider range of the period and robust amplitude for the cell cycle oscillations.

Phase Diffusion and Phase Coherence Associated with the Flux and Energy Cost. A way of quantifying the quality of the limit cycle is through monitoring the phase dynamics and its associated phase coherence time scale. For stochastic dynamics, there is a chance that the phase oscillations may not be coherent. After certain times, the oscillations can lose the memory or track of the previous dynamics. This makes it harder to maintain the periodicity. The phase coherence can be quantified by the time scale involved in the autocorrelation function. $C(t) = \langle X(t)X(t\,)\rangle - \langle X(t)\rangle\langle X(t\,)\rangle$. For the underlying Markovian process, one can fit the correlation function with an exponential, $\langle X(t)X(t\,)\rangle - \langle X(t)\rangle\langle X(t\,)\rangle \exp[-(t-t)/\tau_0]$, or exponentials, where τ_0 represents the time scale of the memory of the phase dynamics. Figure 12a shows the simulated trajectory of the cyclin. We can see that the

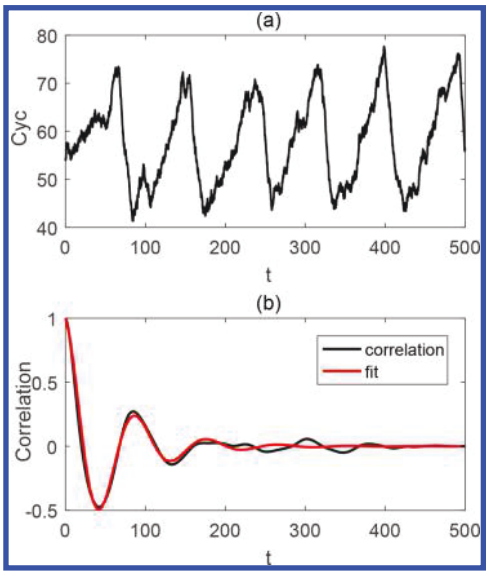

Figure 12. (a) Trajectory of the cyclin. (b) Two-point autocorrelation function and its fit function.

DOI: 10.1021/acs.jpcb.7b11840
J. Phys. Chem. B 2018, 122, 5487−5499

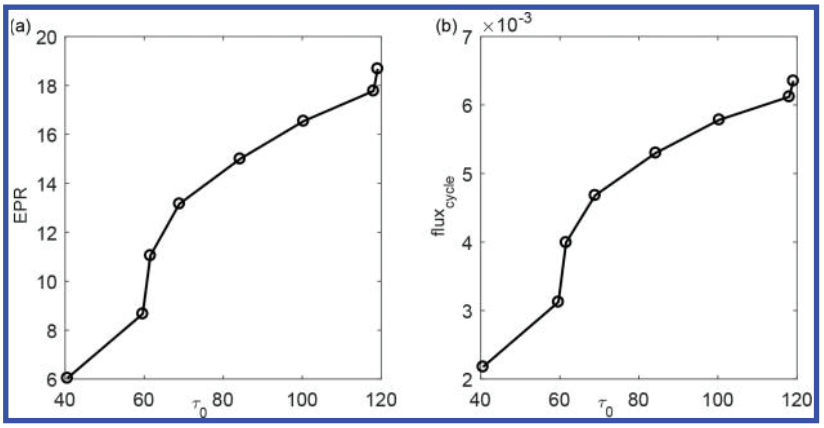

Figure 13. (a) Entropy production rate versus coherence time τ_0. (b) Integral of flux along the limit cycle versus the coherence time τ_0.

oscillation is less robust and inaccurate as a result of the phase fluctuations in the noisy environments. Figure 12b shows the autocorrelation function and its fit function. We can see the autocorrelation function in the network follows a damped oscillation form $C(t) = \exp(-t/\tau_0)\cos(2\pi t/T)$, where τ_0 denotes a coherence time for the oscillation,[43,44] In Figure 13a, we plotted the coherence time τ_0 versus the EPR. Meanwhile, we plotted the coherence time τ_0 versus the flux in Figure 13b. We found that, as the EPR or the flux increases, the coherence time increases. This implies that the flux and energy cost are required for the long coherence of the cell cycle. Due to the phase fluctuations, the cell cycle cannot be perfectly completed in the noisy environments. Longer coherence times can decrease the phase diffusion to sustain the stable and coherent cell cycle. In other words, the energy input can elongate the time scale for coherence memory and therefore the quality of the replication. This prevents the rapid phase diffusion and loss of the phase coherence of the limit cycle. Therefore, the stability and coherence of the cell cycle oscillations come from the flux for driving the dynamics and the input energy cost for sustaining the thermodynamic stability.

Quantifications of the Time Irreversibility and the Flux from the Stochastic Time Traces. A way for quantifying the degree of the detailed balance breaking and time irreversibility is from the differences of the two-point cross correlation function forward and backward in times.[45,46] To show that, one notices that for the cross correlation function can be defined as

$$C_{XY}(\tau) = \langle X(0)Y(\tau)\rangle = \sum X^i Y^j P_i^{ss} P_{ij}(\tau) \tag{1}$$

Here X and Y represent signals. $P_{ij}(\tau)$ is the probability from state i to state j at time τ. P_i^{ss} is the steady state probability being at state i. If the signals X and Y are specific to the states A and B, then

$$C_{XY}(\tau) - C_{YX}(\tau) = X^A Y^B [P_A^{ss} P_{AB}(\tau) - P_B^{ss} P_{BA}(\tau) \tag{2}$$

For a small time interval τ, $\tau P_{ij}(\tau)$ $k_{ij}\tau$ and

$$P_i^{ss} k_{ij} - P_j^{ss} k_{ji} = J_{ij}^{ss} \neq 0 \tag{3}$$

J_{ij}^{ss} is exactly the nonequilibrium steady state probability flux from state i to j. Therefore, the difference between the forward and backward cross correlation functions is directly related to the flux J_{ij}^{ss}

$$C_{XY}(\tau) - C_{YX}(\tau) = X^A Y^B J_{AB}^{ss} \tau \tag{4}$$

and

$$J_{AB}^{ss} = \frac{1}{X^A Y^B} \lim_{\tau\to 0} \frac{C_{XY}(\tau) - C_{YX}(\tau)}{\tau} \tag{5}$$

Therefore, from either the simulated or experimental concentration or expression stochastic trajectories, we can compute the difference in the forward and backward cross correlation functions and obtain the quantitative measure of the time irreversibility and the flux.

Figure 14a shows the simulated trajectories of the cyclin and Cdk1. Figure 14b shows the cross correlation functions

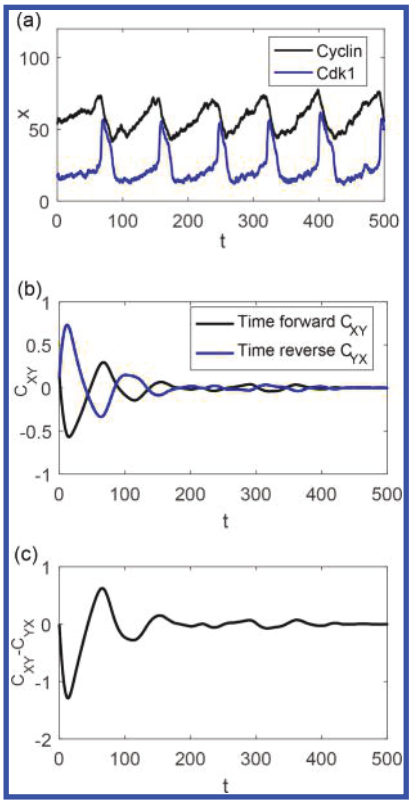

Figure 14. (a) Trajectories of the cyclin and Cdk1. (b) The time forward (black) and time reverse (blue) cross correlation function between the cyclin and Cdk1. (c) The difference of the forward and backward cross correlation functions.

DOI: 10.1021/acs.jpcb.7b11840
J. Phys. Chem. B 2018, 122, 5487−5499

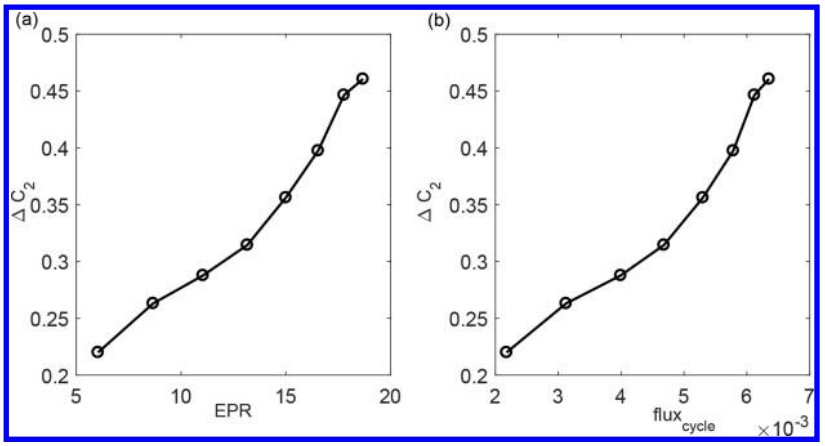

Figure 15. (a) Difference of the forward and backward cross correlation functions ΔC_2 with different entropy production rates. (b) Difference of the forward and backward cross correlation functions ΔC_2 versus the integral of flux along the limit cycle.

between the cyclin and the Cdk1 forward in time and backward in time. Figure 14c shows the difference of the cross correlation functions between the cyclin and the Cdk1 forward in time and backward in time. In Figure 15, we plotted the difference of cross correlation functions ΔC_2 versus the EPR and flux along the limit cycle, where $\Delta C_2 = \sqrt{\frac{1}{t_f}\int_0^{t_f}(C_{XY}(\tau) - C_{YX}(\tau))^2\,d\tau}$ can be used to represent the difference in cross correlation functions between forward in time and backward in time. Since the forward cross correlation function is equal to the backward cross correlation function when the flux is zero, one expects that their nonzero difference measures the degree of the nonequilibrium characterized by the detailed balance breaking through the magnitude of the flux, as mentioned above.[45,46] From Figure 15, indeed we see the difference in cross correlations forward and backward in time is positively correlated to the flux and EPR. Therefore, on the basis of trajectories of the expression or concentrations either from the simulations or the experimental real time traces, we can directly quantify the difference in cross correlations forward and backward in time, from which we can quantify the degree of the time irreversibility and the steady state probability flux for driving the cell cycle flow. The energy input for sustaining the cell cycle gives the emergence of the curl flux for driving the cell cycle dynamics. This breaks explicitly the detailed balance and the time reversible symmetry. Therefore, the degree of the detailed balance breaking and time reversible symmetry breaking are intimately related. They are originated from the energy input manifested in the nonequilibrium dynamics through the curl flux. The time reversal symmetry breaking also creates a stable new phase of active matter, the limit cycle which is supported by the thermodynamic energy input and the dynamical driving from the flux, beyond the equilibrium systems.

CONCLUSIONS

In this study, we explored the underlying mechanisms of the *Xenopus laevis* embryonic cell cycle through uncovering the underlying landscape and flux. First, we quantified the underlying landscape of the cell cycle controlled by the gene regulatory network. The potential landscape has a Mexican hat shape with uneven valleys. Second, we uncovered the relationship between the different phases of the *Xenopus laevis* embryonic cell cycle and the landscape basins on the cycle. We identified the locations and quantified the potential barriers along the oscillation ring as the checkpoints of the *Xenopus laevis* embryonic cell cycle. This provides a physical quantification of the checkpoint mechanism of the *Xenopus laevis* embryonic cell cycle. Third, we uncovered the driving forces for the dynamics of the *Xenopus laevis* embryonic cell cycle, the underlying landscape, and the curl flux which measures the degree of detailed balance breaking. While the landscape leads to the stability of the states on the *Xenopus laevis* embryonic cell cycle, the curl flux drives the persistent oscillation of the *Xenopus laevis* embryonic cell cycle. The potential barriers separate the oscillation into different phases and impede the progression of the cell cycle. Finally, we want to emphasize that the replication is fundamental for biology of living systems. The replication requires a certain energy cost to initiate and sustain in the form of the cell cycle flow. The curl flux originated from the nutrition supply, and the corresponding energy consumption drives and completes the cell cycle process. Our study provides a quantitative statement rather than a qualitative statement on the origin of single cell life. The contribution of the input energy to the cell cycle is quantified by the entropy production rate. The single cell life is quantified by the limit cycle dynamics with the quantified underlying landscape and curl flux for driving the cell cycle dynamics. Energy input/dissipation is shown to be quantitatively correlated to the speed of the cell cycle. This provides the thermodynamic origin of the single cell life as well as the associated sustainability and stability. Curl flux is shown to be quantitatively correlated to the speed of the cell cycle. This provides the dynamical origin of the single cell life in the form of a new active matter phase, and the limit cycle guarantees the associated stable flow. We quantify the quality of the cell cycle by the coherence time and found it is supported by the flux and energy cost. We are also able to quantify the degree of time irreversibility by the cross correlation functions forward and backward in time from the stochastic traces in the simulations or the experiments, providing a way for the quantification of time irreversibility and flux. Through global sensitivity analysis upon landscape and flux, we can identify several key elements for controlling the cell cycle speed. The speed of the cell cycle is a hallmark of cancer. This study can help to design an effective strategy for drug discovery against cancer.

DOI: 10.1021/acs.jpcb.7b11840
J. Phys. Chem. B 2018, 122, 5487−5499

AUTHOR INFORMATION

Corresponding Author

*E-mail: jin.d.wang@gmail.com.

ORCID

Jin Wang: 0000-0002-2841-4913

Notes

The authors declare no competing financial interest.

ACKNOWLEDGMENTS

The authors thank National Nature Science Foundation of China (Grant No. 91430217) and Most, China (Grant No. 2016YFA0203200), for the support. J.W. acknowledges support in part by NSF-PHY-76066. J.W. also thanks Prof. James Ferrell and Prof. Marc Kirschner for helpful discussions.

REFERENCES

(1) Chen, K. C.; Csikasz-Nagy, A.; Gyorffy, B.; Val, J.; Novak, B.; Tyson, J. J. Kinetic analysis of a molecular model of the budding yeast cell cycle. *Mol. Bio Cell* **2000**, *11*, 369−391.

(2) Tyson, J. J.; Novak, B. Regulation of the eukaryotic cell cycle: Molecular antagonism, hysteresis, and irreversible transitions. *J. Theor. Biol.* **2001**, *210*, 249−263.

(3) Chen, K. C.; Calzone, L.; Csikasz-Nagy, A.; Cross, F. R.; Novak, B.; Tyson, J. J. Integrative analysis of cell cycle control in budding yeast. *Mol. Bio Cell* **2004**, *15*, 3841−3862.

(4) Tyson, J. J.; Novak, B. Temporal organization of the cell cycle. *Curr. Biol.* **2008**, *18*, R759−R768.

(5) Goldbeter, A. A minimal cascade model for the mitotic oscillator involving cyclin and cdc2 kinase. *Proc. Natl. Acad. Sci. U. S. A.* **1991**, *88*, 9107−9111.

(6) Qi, H.; Blanchard, A.; Lu, T. Engineered genetic information processing circuits. *WIREs Syst. Biol. Med.* **2013**, *5*, 273−287.

(7) Nurse, P.; Masui, Y.; Hartwell, L. Understanding the cell cycle. *Nat. Med.* **1998**, *4*, 1103−1106.

(8) Swain, P. S.; Elowitz, M. B.; Siggia, E. D. Intrinsic and extrinsic contributions to stochasticity in gene expression. *Proc. Natl. Acad. Sci. U. S. A.* **2002**, *99*, 12795−12800.

(9) Thattai, M.; van Oudenaarden, A. Intrinsic noise in gene regulatory networks. *Proc. Natl. Acad. Sci. U. S. A.* **2001**, *98*, 8614−8619.

(10) Huang, C. Y. F.; Ferrell, J. E. *Proc. Natl. Acad. Sci. U. S. A.* **1996**, *93*, 10078−10083.

(11) Elowitz, M. B.; Leibler, S. A synthetic oscillatory network of transcriptional regulators. *Nature* **2000**, *403*, 335−338.

(12) Ideker, T.; Thorsson, V.; Ranish, J. A.; Christmas, R.; Buhler, J.; Eng, J. K.; Bumgarner, R.; Goodlett, D. R.; Aebersold, R.; Hood, L. Integrated genomic and proteomic analyses of a systematically perturbed metabolic network. *Science* **2001**, *292*, 929−934.

(13) Davidson, E. H.; Rast, J. P.; Oliveri, P.; Ransick, A.; Calestani, C.; Yuh, C. H.; Minokawa, T.; Amore, G.; Hinman, V.; Arenas-Mena, C.; et al. A genomic regulatory network for development. *Science* **2002**, *295*, 1669−1678.

(14) Yu, J.; Xiao, J.; Ren, X. J.; Lao, K. Q.; Xie, X. S. Probing gene expression in live cells, one protein molecule at a time. *Science* **2006**, *311*, 1600−1603.

(15) Kar, S.; Baumann, W. T.; Paul, M. R.; Tyson, J. J. Exploring the roles of noise in the eukaryotic cell cycle. *Proc. Natl. Acad. Sci. U. S. A.* **2009**, *106*, 6471−6476.

(16) Sasai, M.; Wolynes, P. G. Stochastic gene expression as a many-body problem. *Proc. Natl. Acad. Sci. U. S. A.* **2003**, *100*, 2374−9.

(17) Wang, J.; Xu, L.; Wang, E. Potential landscape and flux framework of nonequilibrium networks: robustness, dissipation, and coherence of biochemical oscillations. *Proc. Natl. Acad. Sci. U. S. A.* **2008**, *105*, 12271−6.

(18) Ao, P. Global view of bionetwork dynamics: adaptive landscape. *J. Genet. Genomics* **2009**, *36*, 63−73.

(19) Wang, J.; Li, C.; Wang, E. Potential and flux landscapes quantify the stability and robustness of budding yeast cell cycle network. *Proc. Natl. Acad. Sci. U. S. A.* **2010**, *107*, 8195−200.

(20) Wang, J.; Zhang, K.; Xu, L.; Wang, E. Quantifying the Waddington landscape and biological paths for development and differentiation. *Proc. Natl. Acad. Sci. U. S. A.* **2011**, *108*, 8257−62.

(21) Li, C.; Wang, J. Quantifying cell fate decisions for differentiation and reprogramming of a human stem cell network: landscape and biological paths. *PLoS Comput. Biol.* **2013**, *9*, e1003165.

(22) Van Kampen, N. *Stochastic Processes in Chemistry and Physics*; Elsevier Science B.V. (North-Holland): Amsterdam, The Netherlands, 1992.

(23) Feng, H.; Wang, J. Potential and flux decomposition for dynamical systems and non-equilibrium thermodynamics: curvature, gauge field, and generalized fluctuation-dissipation theorem. *J. Chem. Phys.* **2011**, *135*, 234511.

(24) Qian, H. Mesoscopic nonequilibrium thermodynamics of single macromolecules and dynamic entropy-energy compensation. *Phys. Rev. E: Stat. Phys., Plasmas, Fluids, Relat. Interdiscip. Top.* **2001**, *65*, 016102.

(25) Yang, Q.; Ferrell, J.; E, J. The Cdk1-APC/C cell cycle oscillator circuit functions as a time-delayed, ultrasensitive switch. *Nat. Cell Biol.* **2013**, *15*, 519−25.

(26) Li, C.; Wang, J. Landscape and flux reveal a new global view and physical quantification of mammalian cell cycle. *Proc. Natl. Acad. Sci. U. S. A.* **2014**, *111*, 14130−5.

(27) Gerard, C.; Goldbeter, A. Temporal self-organization of the cyclin/Cdk network driving the mammalian cell cycle. *Proc. Natl. Acad. Sci. U. S. A.* **2009**, *106*, 21643−21648.

(28) Gerard, C.; Goldbeter, A. From simple to complex patterns of oscillatory behavior in a model for the mammalian cell cycle containing multiple oscillatory circuits. *Chaos* **2010**, *20*, 045109.

(29) Gerard, C.; Goldbeter, A. Entrainment of the mammalian cell cycle by the circadian clock:modeling two coupled cellular rhythms. *PLoS Comput. Biol.* **2012**, *8*, e1002516.

(30) Tsai, T. Y.; Choi, Y. S.; Ma, W.; Pomerening, J. R.; Tang, C.; Ferrell, J.; E, J. Robust, tunable biological oscillations from interlinked positive and negative feedback loops. *Science* **2008**, *321*, 126−9.

(31) Minshull, J.; Sun, H.; Tonks, N. K.; Murray, A. W. A map kinase-dependent spindle assembly checkpoint in Xenopus egg extracts. *Cell* **1994**, *79*, 475−486.

(32) Murray, A. W. Cyclin synthesis and degradation and the embryonic-cell cycle. *J. Cell Sci.* **1989**, *1989*, 65−76.

(33) Dart, D. A.; Adams, K. E.; Akerman, I.; Lakin, N. D. Recruitment of the cell cycle checkpoint kinase ATR to chromatin during S-phase. *J. Biol. Chem.* **2004**, *279*, 16433−16440.

(34) Xu, L.; Shi, H.; Feng, H.; Wang, J. The energy pump and the origin of the non-equilibrium flux of the dynamical systems and the networks. *J. Chem. Phys.* **2012**, *136*, 165102.

(35) Zhang, K.; Sasai, M.; Wang, J. Eddy current and coupled landscapes for nonadiabatic and nonequilibrium complex system dynamics. *Proc. Natl. Acad. Sci. U. S. A.* **2013**, *110*, 14930−5.

(36) Yoda, M.; Ushikubo, T.; Inoue, W.; Sasai, M. Roles of noise in single and coupled multiple genetic oscillators. *J. Chem. Phys.* **2007**, *126*, 115101.

(37) Izumi, T.; Walker, D. H.; Maller, J. L. Periodic changes in phosphorylation of the Xenopus cdc25 phosphatase regulate its activity. *Mol. Bio Cell* **1992**, *3*, 927−939.

(38) Kumagai, A.; Dunphy, W. G. Regulation of the cdc25 protein during the cell-cycle in Xenopus extracts. *Cell* **1992**, *70*, 139−151.

(39) Yoshida, T.; Tanaka, S.; Mogi, A.; Shitara, Y.; Kuwano, H. The clinical significance of Cyclin B1 and Wee1 expression in non-small-cell lung cancer. *Ann. Oncol* **2004**, *15*, 252−256.

(40) Novak, B.; Tyson, J. J. Modeling the cell-division cycle - M-Phase trigger, oscillations, and size control. *J. Theor. Biol.* **1993**, *165*, 101−134.

(41) Georgi, A. B.; Stukenberg, P. T.; Kirschner, M. W. Timing of events in mitosis. *Curr. Biol.* **2002**, *12*, 105−114.

DOI: 10.1021/acs.jpcb.7b11840
J. Phys. Chem. B 2018, 122, 5487−5499

(42) Trunnell, N. B.; Poon, A. C.; Kim, S. Y.; Ferrell, J. E. Ultrasensitivity in the regulation of cdc25C by cdk1. *Mol. Cell* **2011**, *41*, 263−274.
(43) Cao, Y.; Wang, H.; Ouyang, Q.; Tu, Y. The free-energy cost of accurate biochemical oscillations. *Nat. Phys.* **2015**, *11*, 772−778.
(44) Potoyan, D. A.; Wolynes, P. G. On the dephasing of genetic oscillators. *Proc. Natl. Acad. Sci. U. S. A.* **2014**, *111*, 2391−6.
(45) Qian, H.; Elson, E. L. Fluorescence correlation spectroscopy with high-order and dual-color correlation to probe nonequilibrium steady states. *Proc. Natl. Acad. Sci. U. S. A.* **2004**, *101*, 2828−33.
(46) Li, C.; Wang, E.; Wang, J. Landscape, flux, correlation, resonance, coherence, stability, and key network wirings of stochastic circadian oscillation. *Biophys. J.* **2011**, *101*, 1335−44.

DOI: 10.1021/acs.jpcb.7b11840
J. Phys. Chem. B 2018, 122, 5487−5499